

InfNeRF: Towards Infinite Scale NeRF Rendering with $O(\log n)$ Space Complexity

JIABIN LIANG*, Sea AI Lab, Singapore
 LANQING ZHANG, Sea AI Lab, Singapore
 ZHUORAN ZHAO, National University of Singapore, Singapore
 XIANGYU XU, Xi'an Jiaotong University, China

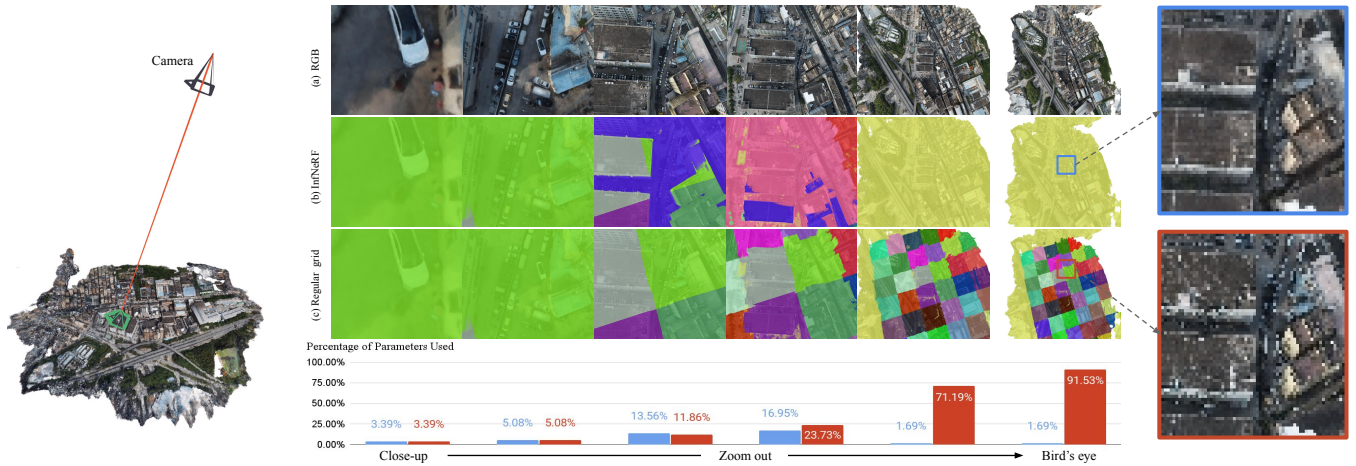


Fig. 1. Efficient large-scale scene rendering with the proposed InfNeRF. (a) shows the rendered RGB frames by InfNeRF under a zoom-out camera trajectory. Unlike existing methods that employ regular grid partition at a single scale (c), we propose a hierarchical NeRF framework to decompose the scene in both space and scale dimensions (b), in a spirit similar to the classical LoD techniques. This innovation is color-coded in (b) and (c), with each color representing a unique NeRF node within the whole model. During rendering, InfNeRF only requires a fraction of the nodes, considerably diminishing the memory footprint and expediting the model retrieval process. As demonstrated in the middle bottom chart, a mere maximum of 16.95% parameters of the entire model are used for the rendering of InfNeRF, in stark contrast to the 91.53% demanded by the baseline approach. In addition to the improved storage efficiency, the hierarchical structure of InfNeRF naturally improves its anti-aliasing capability. As shown in the rightmost column, InfNeRF shows notably reduced noise and enhanced smoothness while the existing methods suffer from severe aliasing artifacts.

The conventional mesh-based Level of Detail (LoD) technique, exemplified by applications such as Google Earth and many game engines, exhibits the capability to holistically represent a large scene even the Earth, and achieves rendering with a space complexity of $O(\log n)$. This constrained data requirement not only enhances rendering efficiency but also facilitates dynamic data fetching, thereby enabling a seamless 3D navigation experience for users.

In this work, we extend this proven LoD technique to Neural Radiance Fields (NeRF) by introducing an octree structure to represent the scenes in different scales. This innovative approach provides a mathematically simple and elegant representation with a rendering space complexity of $O(\log n)$,

*Corresponding author.

Permission to make digital or hard copies of all or part of this work for personal or classroom use is granted without fee provided that copies are not made or distributed for profit or commercial advantage and that copies bear this notice and the full citation on the first page. Copyrights for components of this work owned by others than the author(s) must be honored. Abstracting with credit is permitted. To copy otherwise, or republish, to post on servers or to redistribute to lists, requires prior specific permission and/or a fee. Request permissions from permissions@acm.org.

SA Conference Papers '24, December 3–6, 2024, Tokyo, Japan

© 2024 Copyright held by the owner/author(s). Publication rights licensed to ACM.

ACM ISBN 979-8-4007-1131-2/24/12...\$15.00

<https://doi.org/10.1145/3680528.3687646>

aligned with the efficiency of mesh-based LoD techniques. We also present a novel training strategy that maintains a complexity of $O(n)$. This strategy allows for parallel training with minimal overhead, ensuring the scalability and efficiency of our proposed method. Our contribution is not only in extending the capabilities of existing techniques but also in establishing a foundation for scalable and efficient large-scale scene representation using NeRF and octree structures. Code and checkpoints are available at: <https://jiabinliang.github.io/InfNeRF.io/>

CCS Concepts: • **Computing methodologies** → **Reconstruction; Rendering; Volumetric models; Antialiasing.**

Additional Key Words and Phrases: novel view synthesis, radiance fields, level of detail,

ACM Reference Format:

Jiabin Liang, Lanqing Zhang, Zhuoran Zhao, and Xiangyu Xu. 2024. InfNeRF: Towards Infinite Scale NeRF Rendering with $O(\log n)$ Space Complexity. In *SIGGRAPH Asia 2024 Conference Papers (SA Conference Papers '24)*, December 3–6, 2024, Tokyo, Japan. ACM, New York, NY, USA, 10 pages. <https://doi.org/10.1145/3680528.3687646>

1 INTRODUCTION

Recent progress in Neural Radiance Fields (NeRF) has significantly advanced the field of photo-realistic novel-view synthesis [Barron et al. 2021, 2023; Mildenhall et al. 2021]. Surpassing traditional 3D representations like meshes, NeRF demonstrates a superior capability in generating accurate novel views, particularly for transparent or reflective geometries. However, despite these advancements, a predominant focus of NeRF research has been confined to single objects or limited-scale scenes. The challenge of effectively representing extensive, large-scale scenes remains largely underexplored and unresolved.

Large-scale scene reconstruction has a wide range of applications, such as land surveys, search and rescue operations, construction planning, and navigation. A prime example of its potential can be seen in platforms like Google Earth, enabling users to virtually traverse the globe, which not only showcases the magnificent beauty of natural landscapes but also facilitates the exploration of intricate historic buildings. Extending NeRF to handle large-scale scenes is intriguing and important because it opens up possibilities for more immersive and realistic representations of our world.

1.1 Block-NeRF and Mega-NeRF

Simply scaling up the architecture of NeRF proves insufficient to address this challenge, primarily due to the escalating space complexity. As the scenes expand, it becomes impractical to store the entire model in the memory of standard devices such as mobile phones or consumer PCs. Consequently, dividing the model and storing it in disk or cloud systems becomes necessary.

Towards this direction, recent large-scale NeRF approaches, such as Block-NeRF [Tancik et al. 2022] and Mega-NeRF [Turki et al. 2022] divide the whole neural field equally in space into smaller, more manageable blocks, referred to as grid partition in this paper. This allows the rendering device to load only the data relevant to the camera’s current location. However, these methods encounter challenges in scenarios requiring a bird’s eye view of the entire scene. Such a panoramic view plays a crucial role in human interactive navigation. For example, to adjust the position of the camera, it is much more efficient to first zoom out, identify the target location, and then zoom in again, compared to the laborious process of navigating at a constant zoomed-in level. In such scenarios, the existing methods need to load all blocks simultaneously, which can overwhelm the memory capacity of the device. In addition to the memory issue, these approaches are prone to aliasing artifacts that arise from an insufficient sampling rate for high-frequency signals as illustrated in Fig. 1.

1.2 Proposed InfNeRF

In this paper, we propose InfNeRF, a novel method that addresses the above challenges. The core concept of InfNeRF is inspired by the classical mesh-based Level of Detail (LoD) techniques [Clark 1976; Erikson et al. 2001; Ribelles et al. 2010; Tanner et al. 1998]. An overview is illustrated in Fig. 2. Specifically, we construct a LoD tree for the target scene, where each node encapsulates a small NeRF with a roughly equivalent number of parameters. The root node provides a coarse representation of the entire scene, while

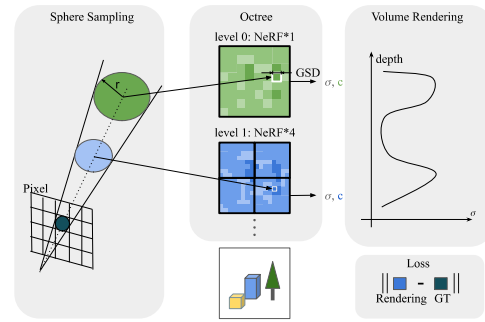


Fig. 2. Each sampling sphere along the ray is assigned a radius corresponding to its pixel size. The radius is proportional to depth. Depending on the radius, the sampling spheres will be sent to different nodes of the octree to query their densities and colors. The densities and colors are integrated using volume rendering to produce the final color for the pixel.

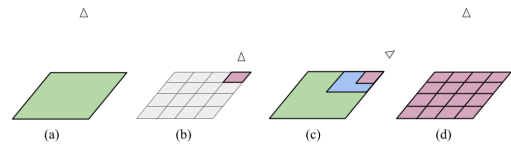


Fig. 3. As illustrated in (a), when zooming out, only the root node is required. In (b), when zooming in, only the leaf node is required. In (c), when looking at the horizon, approximately $O(\log n)$ nodes are required which is the upper bound of InfNeRF. In (d), in contrast, other methods require all the blocks when zoom out resulting in an upper bound of $O(n)$.

its successive children progressively describe more detailed sub-regions. During rendering, each sampling point is forwarded by a different NeRF, depending on its location and radius. The density and color then are accumulated to determine the pixel color.

As illustrated in Fig. 3, InfNeRF only requires a minimum subset of the nodes in rendering, chosen based on their proximity to the camera and their intersection within the frustum. This significantly reduces the memory burden and the I/O time for retrieving parameters from disk or cloud storage. The memory complexity is notably efficient at $O(\log n)$, where n denotes the total information captured in the reconstruction. In the real world, with $\log n \approx 20$, we can represent the Earth down to a resolution of centimeters. In general, InfNeRF is like the combination of Mega-NeRF [Turki et al. 2022] and PyNeRF. It divides the scene in both spatial and scale dimensions while existing approaches typically only consider one of them.

Another remarkable feature of InfNeRF is that the parent nodes in the LoD tree act as a smoother, low-pass-filtered version of the scene. Therefore, the proposed method naturally removes high-frequency components in distant views, which effectively reduces the aliasing artifacts and enhances the visual quality of the generated images (Fig. 1). In our experiments, InfNeRF achieves superior rendering quality for large-scale reconstruction, with an improvement of over 2.4 dB in PSNR while accessing only 17% of the total parameters.

We also propose a pruning algorithm to prune the octree into an effective and compact representation using sparse points from SfM. This algorithm adapts the tree to each scene intelligently without any human intervention.

In addition, the training of InfNeRF only increases slightly and maintains a time and space complexity of $O(n)$. Moreover, this strategy allows for the training process to be effectively parallelized across machines.

InfNeRF imposes no constraints on the underlying NeRF model and makes no assumptions about the scene, making it an adaptable framework that can seamlessly accommodate and leverage the rapid advancements in NeRF models.

In summary, our contributions are as follows:

- We propose a novel InfNeRF for large-scale scene reconstruction. By integrating neural fields with the classic LoD, InfNeRF achieves efficient rendering with a significantly reduced memory footprint.
- Our InfNeRF demonstrates a substantial improvement in rendering quality, with over 2.4 dB increase in PSNR, and exhibits superior anti-aliasing capabilities.
- We develop an efficient and scalable training strategy tailored for InfNeRF, addressing the complexities inherent in large-scale neural field training.

2 RELATED WORK

2.1 Photogrammetry

Among the established reconstruction techniques, mesh-based reconstruction methods called photogrammetry have been used widely for its efficiency and robustness in creating digital twins world. Open-source tools, such as COLMAP [Schonberger and Frahm 2016] and OpenMVS [Cerneja 2020], have seamlessly integrated this workflow and gained widespread adoption in the academic community. Furthermore, commercial software solutions like ContextCapture and DJI Terra [DJI 2024] have significantly elevated the robustness and efficiency to meet industrial standards.

2.2 Level of Detail

When the scene is large, it becomes impractical to store it entirely in memory. In this case, the Level of Detail (LoD) or Hierarchical Level of Detail (HLoD) [Clark 1976; Erikson et al. 2001; Hoppe 1998, 2023; Luebke 2003; Ulrich 2002] provides a framework for efficiently storing, fetching, and rendering the scene.

Take tiled 2D map [Tiled web map 2024] used widely in 2D navigation system for an example. The maps in different resolutions are cut into 256×256 PNG images referred to as tiles. These tiles are organized into a quadtree structure, typically comprising 22 levels. This hierarchical arrangement allows web browsers to rapidly fetch data and render any location at any zoom level with constant space complexity.

A similar technique can also be applied to 3D mesh. After the reconstruction of the scene into one detailed mesh, this mesh undergoes multiple simplifications [Daniels et al. 2008] to reduce the number of triangles. Concurrently, its texture also undergoes down-sampling multiple times [Williams 1983]. Together this results in a mesh pyramid with varying levels of detail, ranging from fine to

coarse. Subsequently, these meshes are partitioned into numerous tiles and organized hierarchically, resembling a tree structure similar to a quadtree in 2D mapping. During rendering, 3D engine such as CesiumJS [CesiumJS 2024] or OpenSceneGraph [Burns and Osfield 2004] walks the tree, then progressively fetch tiles based on their proximity and intersection with the frustum. This LoD technique enables users to have a seamless 3D navigation experience in a very large scene while maintaining a low memory footprint.

2.3 NeRF

NeRF [Mildenhall et al. 2021] employs Multi-Layer Perceptrons (MLPs) for NeRF to capture a continuous density and viewpoint-dependent radiance of a scene. Methods like TensorRF [Chen et al. 2022] and MERF [Reiser et al. 2023] decompose the dense grid into low dimension feature tensor, while InstantNGP [Müller et al. 2022] opts to store these vectors in a sparse hash table. These strategies greatly enhance model compactness while maintaining speed.

2.4 Large-Scale Scene and Partition at Space Dimension

While previous NeRF approaches primarily focus on scenes of limited scale, scaling up NeRF to handle large-scale scenes, such as cities or even the entire Earth, would empower a broader range of applications. Mip-NeRF 360 [Barron et al. 2022] proposed a scene contraction technique to compress the unbounded scene into a bounded region. However, this approach compromises quality in the compressed areas. Grid-Guided NeRF [Xu et al. 2023] extends its capacity by combining a 2D feature grid and MLP, but its reliance on a 2D plane assumption limits its capability to handling complicated 3D scene. Block-NeRF [Tancik et al. 2022], Mega-NeRF [Turki et al. 2022], SMERF [Duckworth et al. 2023] and ScaNeRF [Wu et al. 2023] divide the scene into several sub-regions and reconstruct them separately. In its specialized indoor scenario, SMERF can even achieve impressive real-time rendering. However, all these methods suffer from a common issue: when rendering a bird's eye view, the entire model has to be loaded into VRAM, limiting their scalability. Additionally, they may suffer from severe aliasing artifacts.

2.5 Anti-aliasing and Partition at Scale Dimension

Anti-aliasing has been a fundamental problem in computer graphics and image processing for a long time and has been extensively explored in the rendering community. The common approaches to tackle this problem can be categorized into two ways: super-sampling and pre-filtering. In the context of NeRF, super-sampling is casting multiple rays per pixel as in MobileNeRF [Chen et al. 2023], or sampling multiple points with perturbation, as demonstrated in Zip-NeRF [Barron et al. 2023]. This straightforward strategy is useful but also computationally expensive. On the other hand, Mip-NeRF [Barron et al. 2021] introduces the concept of pre-filtering through the integrated position encoding. Other research has explored scene partitioning at different scales to mitigate aliasing. For instance, BungeeNeRF [Xiangli et al. 2022] proposes a multi-scale MLP that progressively adds detail when the camera zooms in. Tri-MipRF [Hu et al. 2023a], PyNeRF [Turki et al. 2023] and Mip-VoG [Hu et al. 2023b] train a multi-resolution feature grid. These

methods demonstrate impressive anti-aliasing capabilities and consistently high-quality rendering across the entire scene. However, their lack of space partitioning leads to challenges when scaling up, requiring the whole finest layer to render a close-up frame.

In contrast to the methods mentioned in this subsection, the anti-aliasing problem is addressed with inherently no additional cost in InfNeRF. Our parent node in the octree is a downsampled copy of the child nodes. Rendering these nodes at an appropriate zoom level yields a result free from aliasing artifacts.

2.6 Scene Partition with an Octree

Some researches, like PlenOctrees [Yu et al. 2021] and NGLoD [Takikawa et al. 2021] utilize an octree-based approach to represent the scene. PlenOctrees stores the spherical harmonics coefficients in the leaves and uses the octree to accelerate accessing, while in NGLoD, a signed distance field is stored in the octree to represent a LoD closed volume. These direct storage techniques provide fast access and training but require significant memory, limiting their scalability. In contrast, InfNeRF employs many compact hash tables as the underlying data storage. The shallow octree is primarily used for organizing the hash tables into a LoD structure. This approach results in a much more compact LoD representation and much better scalability.

2.7 Gaussian Splatting

In recent times, Gaussian splatting [Kerbl et al. 2023] has gained significant attention due to its fast rendering speed compared to NeRF. Additionally, the introduction of Mip-Splatting [Yu et al. 2024] effectively reduces aliasing artifacts across different resolutions. Then Hierarchical Gaussians [Kerbl et al. 2024], VastGaussian [Lin et al. 2024], and CityGaussian [Liu et al. 2024], explore its potential in large scene reconstruction. While Gaussian splatting may not achieve the same PSNR as traditional NeRF [Liu et al. 2024] in challenging scenarios such as varying light conditions or camera exposure, it remains a promising technique for large-scale scene reconstruction in the future.

3 METHOD

We present InfNeRF, a framework for efficient large-scale scene reconstruction using a LoD octree structure (Section 3.1). This tree structure naturally enables anti-aliasing rendering (Section 3.2), which significantly enhances the visual quality of rendered images. We also introduce tree pruning to improve model sparsity and compactness, along with a rendering approach tailored for the pruned structure (Section 3.3). Moreover, we propose an efficient training strategy for InfNeRF in Section 3.4. Finally, we provide a comprehensive analysis of the computational complexity of InfNeRF in supplementary material, offering insights into the efficiency and scalability of our approach in handling large-scale scene reconstructions.

3.1 Tree Structure

The core of our InfNeRF is a LoD structure, essentially an octree where each node represents a specific cubic space of the scene, known as the node’s Axis-Aligned Bounding Box (AABB). The octree is illustrated in the middle of Fig. 2. InfNeRF begins with the

entire scene encapsulated within a root node, which is then divided into eight smaller cubes, corresponding to the child nodes. This division process continues recursively, partitioning the scene into increasingly finer parts, both in terms of space (size of the area) and scale (level of detail).

Each node in this tree is paired with its own NeRF, which represents the node’s AABB at a certain scale. Our approach is flexible regarding the choice of NeRF model. It can be a simple MLP [Mildenhall et al. 2021], Instant-NGP [Müller et al. 2022], triplane [Chan et al. 2022; Hu et al. 2023a], or even a combination of them, as long as it can query the density σ and the color \mathbf{c} for a given 3D point \mathbf{x} and viewing direction \mathbf{d} :

$$\sigma, \mathbf{c} = \text{NeRF}(\mathbf{x}, \mathbf{d}). \quad (1)$$

In this work, we use Instant-NGP for its efficiency in training. Instant-NGP discretizes each cube into a grid of voxels, and the number of voxels along each axis of the cube is defined as grid size. Correspondingly, the Ground Sampling Distance (GSD) of a node can be approximated as:

$$\text{GSD} = \frac{\text{length of AABB}}{\text{grid size}}, \quad (2)$$

whose unit is in meters. The GSD, in this context, serves as a measure of resolution or granularity, indicating the level of detail that the node can capture about the physical world - the smaller the GSD, the finer the details. For example, if a node \mathcal{A} represents a 1 km^3 cube with a grid size of 2048, the GSD will be $\frac{1000}{2048} \approx 0.48$ meters. As each node in our octree shares the same grid size, the child nodes of \mathcal{A} have a GSD of 0.24 meters, thereby capturing more detailed information. This is also illustrated in Fig. 2, where the GSD of a cube at level 1 is half that of a cube at level 0.

3.2 Anti-Aliasing Rendering

Similar to the original NeRF, the rendering process of InfNeRF accumulates the density and color of sampling points along a ray to determine the RGB of a pixel. However, the key difference is that the sampling points are queried from different nodes of our octree as shown in Fig. 2 rather than a single NeRF. In the following, we show how we find the corresponding node for a given sampling point.

According to the sampling theory [Williams 1983], a sample on the ray is not merely an infinitely small point, but rather a Gaussian sphere with a certain volume. For simplicity, we model this as a sphere with radius r that corresponds to the pixel size,

$$r \approx \text{depth} \times \frac{\text{pixel width}}{2 \times \text{focal length}}, \quad (3)$$

as illustrated on the left of Fig. 2. Then, given a sampling sphere with position $\mathbf{x} \in \mathbb{R}^3$ and radius $r \in \mathbb{R}$, we aim to find the node whose granularity (GSD) matches r and whose AABB contains \mathbf{x} . In this way, we ensure InfNeRF samples a proper region in the 3D space rather than just a single point, leading to a desirable anti-aliasing effect.

We observe that when the sampling sphere falls between two discrete levels, small aliasing occurs. Nevertheless when sampling points transition between levels, discrepancies in density or color

may arise, engendering an undesirable "popup" effect when camera moves. To mitigate these phenomenons, both PyNeRF and TriMipRF employ interpolation techniques between adjacent levels which will double the computation. However, we pursue a simpler approach by introducing stochastic perturbations to the radius of the sampling sphere.

$$r_{prt} = r \times 2^p, \text{ where } p \sim \mathcal{U}(-0.5, 0.5). \quad (4)$$

This strategy use human eye's natural blending effect to attenuate the abrupt transitions without incurring additional computational cost. Finally, the level to sample a given sphere is determined by:

$$\text{level} = \lfloor \log_2 \frac{\text{root.gsd}}{r_{prt}} \rfloor, \quad (5)$$

where root.gsd denotes the GSD of the root node, *i.e.*, level 0.

As illustrated in Fig. 3(a), when the camera is far away from the scene, all spheres are relatively large, and therefore, their densities and colors are estimated by the root node, resulting in a smooth anti-aliasing effect. Conversely, as shown in Fig. 3(b), zooming in with the camera reduces the size of the spheres, which shifts the estimation to the leaf nodes, yielding a sharp and detailed image. As InfNeRF necessitates only a minimum subset of the nodes for rendering a frame, it requires loading merely $O(\log n)$ number of parameters from the whole model into memory. The upper bound $O(\log n)$ is reached when the camera looks at the distant horizon, as illustrated in Fig. 3(c). In this scenario, multiple-level nodes are engaged simultaneously, from the root node representing the blurring horizon to the leaf node representing foreground details.

3.3 Tree Pruning

While we can build a perfect octree as in Section 3.1, this may not be efficient, particularly for non-uniformly sampled scenes. To optimize the structure, it is important to identify the essential nodes necessary for rendering all input images, effectively pruning the superfluous parts of the tree.

In this work, we utilize sparse points $\mathbf{x} \in \mathbb{R}^3$ obtained from the Structure from Motion (SfM) to approximate scene geometry. Each sparse point \mathbf{x}_i observed in M_i images is treated as M_i spheres, each with a radius $r_{ij}, j = 1, \dots, M_i$ as defined in Section 3.2. We find the corresponding nodes for all the $\sum M_i$ spheres in an ideal, infinitely deep octree as described in Section 3.2. We retain only the nodes that correspond to sparse spheres and their respective parent nodes, while the others are pruned away.

Compared to Mega-NeRF or Block-NeRF, which split the scene uniformly based on space occupancy, our approach offers a more intelligent resource allocation strategy. It adaptively creates deeper branches in areas with rich details and shallower branches in coarse regions.

This approach is robust as the subtree pruning is only restricted to cases where there are no sparse points in a relatively large cube. As further detailed below, even in the rare case that a subtree is pruned by mistake, like in low texture area, the affected volume can still be well reconstructed by its parent node, albeit in a coarser manner. This ensures that, while fine details may be omitted, the essential structure is preserved.

3.3.1 Pruned Tree Rendering. The pruned tree structure introduces new challenges in InfNeRF rendering, as the optimal node determined by Eq. 5 may no longer exist after pruning. In such scenarios, we instead process the sampling sphere with the nearest available ancestor of the intended node.

Specifically, given a sampling sphere (\mathbf{x}, r) , the rendering process recursively travels down the tree. If the sphere successfully arrives at the node of the expected level, the density and color of the sphere will be estimated by that node. However, if this process is interrupted by a pruned node, the rendering of the sphere reverts to its parent node. We outline this rendering strategy with the pseudo-code in Algorithm 1. The additional computational overhead introduced by tree traversal includes $\log(n)$ times floating-point comparisons and memory reads, which can be considered negligible when compared to the NeRF evaluation.

Algorithm 1: Forward run of the pruned tree in Section 3.3, starting from $\text{node} = \text{root}$.

```

Input: node
Input:  $\mathbf{x}, r, \mathbf{d} \leftarrow \text{position, radius, direction}$ 
Output: density, color
Function Forward( $\text{node}, \mathbf{x}, r, \mathbf{d}$ ):
  if  $r \geq \text{node.gsd}$  then
    | return  $\text{node.NeRF}(\mathbf{x}, \mathbf{d})$ ; //Process
  else
    |  $i \leftarrow \text{FindSubcube}(\text{node.AABB}, \mathbf{x})$ ;
    |  $\text{child} \leftarrow \text{node.children}[i]$ ;
    | if  $\text{child} = \text{nil}$  then
    | | return  $\text{node.NeRF}(\mathbf{x}, \mathbf{d})$ ; //Revert
    | else
    | | return Forward( $\text{child}, \mathbf{x}, r, \mathbf{d}$ ); //Descend
  end
end

```

3.4 Training

3.4.1 Training Loss. To train the proposed InfNeRF, we accumulate the density and color of all spheres sampled on a ray using volume rendering [Mildenhall et al. 2021] and compare the resulting RGB values with the pixels of the observed images using L2 loss \mathcal{L}_{RGB} . To remove the cloudy effect from the unobserved areas, particularly in the sky, and enhance visual quality in the bird's-eye view, we introduce a transparency loss $\mathcal{L}_{\text{trans}} = -\|\exp(-\sigma(\mathbf{x}))\|_1$, which uniformly samples points within the AABB and uses L1 loss to encourage their density to approach 0.

To further improve the result, we also incorporate the distortion loss $\mathcal{L}_{\text{distort}}$ from [Barron et al. 2022] and a regularization loss \mathcal{L}_{reg} who measures the L2 differences of the density between levels, to promote the density consistency. The total loss of our training is summarized as:

$$\mathcal{L}_{\text{total}} = \mathcal{L}_{\text{RGB}} + w_1 * \mathcal{L}_{\text{distort}} + w_2 * \mathcal{L}_{\text{reg}} + w_3 * \mathcal{L}_{\text{trans}} \quad (6)$$

3.4.2 Pyramid Supervision. The images in our datasets are captured by drones at relatively close proximity, resulting in a lack

of multi-resolution information necessary to supervise the higher-level nodes. To mitigate this issue, following PyNeRF [Turki et al. 2023]’s approach, we augment the training set using an image pyramid constructed by repeatedly downsampling the high-resolution images. The lower-resolution image with a larger pixel size, create larger sampling spheres according to Eq. 3. These larger sampling spheres are sampled from higher-level nodes in the octree, effectively supervising their training. To account for the pixel imbalance across different pyramid levels, we perform uniform sampling in pixel domain, where a high-resolution image receives four times the sampling rate compared to its low-resolution counterpart. This strategy facilitates more balanced training across different levels of the image pyramid.

3.4.3 Distributed Training. As the scene grows, the demands on VRAM and training time also increases. Straightforwardly using existing distributed training approaches, such as Distributed Data Parallel (DDP), leads to increased VRAM consumption and substantial communication overhead. To address these limitations, we propose a new distributed training strategy.

Given a specific tree level $L \in \mathbb{Z}^+$, we split the octree into two parts: the upper tree which includes all nodes from level 0 to level $L - 1$, and the lower part which is a forest including a maximum of 8^L subtrees. During training, the upper tree is shared across all devices, and the parameters are updated concurrently. Meanwhile, individual subtrees are assigned among different devices and updated independently. In other words, each device only maintains the shared upper tree and a subset of the lower subtrees, effectively reducing the VRAM footprint and communication overhead. For instance, let’s consider a perfect octree with four levels. When the root node is shared ($L = 1$), the shared upper tree contains only a tiny fraction, approximately 0.17%, of all the parameters in the entire tree. During forward pass, if a sampling sphere descends to a subtree that is not owned by the current device, it will be forwarded by its parent node in the shared tree as demonstrated in Fig. 4. Consequently, during training, the only data transfer is the all-reduce operation on the gradient of the shared upper tree, which leads to a more efficient and scalable training process.

Furthermore, the training data can also be divided among devices for further acceleration. Intuitively, if a ray on a particular device does not intersect with the AABB of any subtree on that device, it would be not sensible to sample the corresponding pixel of the ray. Therefore, we find a 2D AABB for each device by projecting the sparse points inside the subtrees’ 3D AABBs back onto images. Then, during the training phase, only the pixels that fall within the 2D AABB are sampled and utilized. The experimental result of distribution training is provided in supplementary materials.

4 EXPERIMENT

InfNeRF is implemented using the NeRFStudio framework [Tancik et al. 2023]. Each node’s NeRF is an Instant-NGP with default parameters such as a grid size of 2048 and 16 levels of hash tables, each with a size of 2^{19} . Following NeRF-w [Martin-Brualla et al. 2021], each image is assigned an appearance embedding vector $e \in \mathcal{R}^{32}$ to encode its lighting condition. More implementation details such as

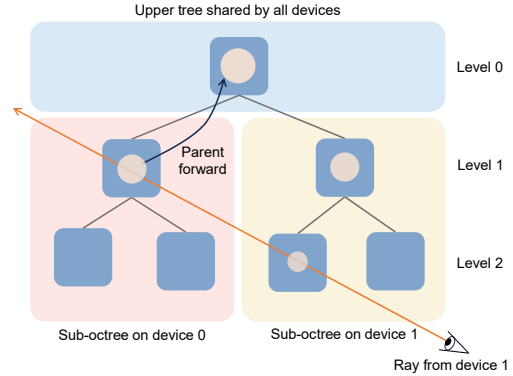


Fig. 4. Illustration of the distributed octree as a binary tree for simplicity. The tree can be divided into the root and 2 branches. The root is shared by all devices like Conventional DDP. And each branch is owned by one device without sharing the weights. When a sampling sphere descends to a pruned node, its density and color will be estimated by the shared parent node.

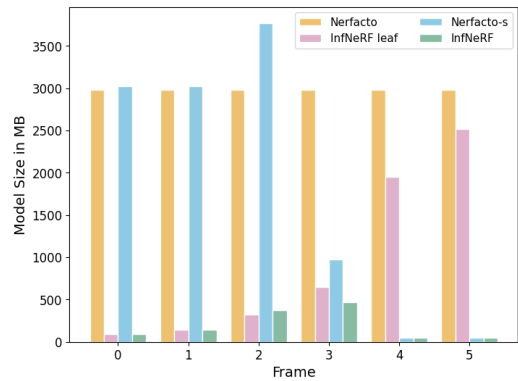


Fig. 5. We render a video starting from a close-up view and zooming out to the full scene and report the size of all sub NeRFs required for rendering each frame. Thanks to the LoD tree structure, InfNeRF demonstrated a much smaller memory footprint.

learning rate and experiment settings are provided in supplementary materials.

4.1 Experiment On Large-Scale Dataset

4.1.1 Dataset. To evaluate the scalability of our method, we adopt a similar approach to Mega-NeRF [Turki et al. 2022], by conducting our main experiment using four real-world large-scale urban scenes dataset captured by drone from Mill 19 [Turki et al. 2022] and UrbanScene3D [Lin et al. 2022]. Each dataset consists of around two thousand 4K images, amounting to 40 gigapixels and spanning 1 km. Notably, they are approximately 200 times larger than the scenes reported in other general NeRF work. Our octree is limited to 4 levels, resulting a reasonable GSD ranges from 0.4 m of the root node to 5 cm of the leaf node. The total model size is about 3 GB.

4.1.2 Result on Space Complexity. The paramount objective of our study is to reduce the required model size in rendering, which

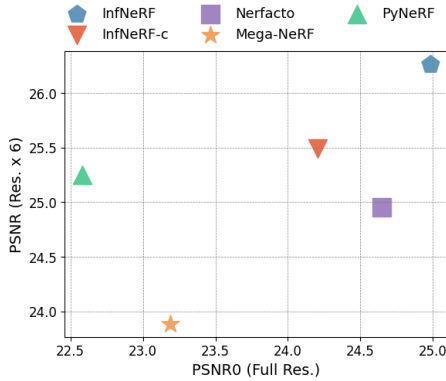


Fig. 6. The PSNR for full resolution and across 6 resolutions of 4 methods are presented in the above plots. InfNeRF is superior to other methods in both dimensions.

refers to the sum of all sub NeRFs’ size required for rendering one frame. It is the total information that needs to be retrieved from the clouds and stored in the local device during real-time rendering. To demonstrate the impact of our octree on the required model size, we compare InfNeRF with three other methods with similar total model sizes but with different architectures. These three methods are: (1) Nerfacto [Tancik et al. 2023], (2) Nerfacto-s, a 4 levels Nerfacto, representing the scale partition methods like PyNeRF [Turki et al. 2023], (3) InfNeRF leaf, an InfNeRF without upper tree structure, representing the space partition methods like Mega-NeRF [Turki et al. 2022].

In this experiment, we examine the rendering of a zoom-out trajectory, starting from a close-up view and transitioning to a bird’s-eye view in VGA resolution. The trajectory and the corresponding rendered images are shown in Fig. 1. We present the required model size in megabytes for six keyframes in Fig. 5. When rendering the close-up view, the space partition method InfNeRF leaf proves advantageous as it only requires a single node of the scene and has low space requirements. In contrast, the scale partition methods Nerfacto-s necessitate the detailed version of the entire scene, resulting in a higher space complexity. As the camera moves away, the space partition method InfNeRF leaf now requires all blocks to render the complete scene, while the scale partition method reduces its requirement by only rendering the low-resolution node. However, InfNeRF consistently exhibits its low space complexity in both scenarios, with a memory footprint of only 17% compared to InfNeRF leaf and 12.3% compared to Nerfacto-s.

4.1.3 Result on Rendering Quality. As zoom-out is a crucial use case in our paper, we not only report metrics at the finest resolution, denoted as PSNR0, but more importantly, the mean metrics over 6 resolution levels, denoted as PSNR, SSIM, LPIPS. We compare our approach with (1) Nerfacto [Tancik et al. 2023], whose model size is scaled up to InfNeRF, (2) PyNeRF [Turki et al. 2023], also being scaled up to InfNeRF, (3) Mega-NeRF [Turki et al. 2022] with 25 partitions, (4) InfNeRF compact (InfNeRF-c), whose model size is similar to Mega-NeRF.

The PSNR0 (full resolution) and all 3 metrics for multi-resolution are listed in Table 1. The mean across the four datasets are also plotted in Fig. 6. When comparing two models with similar model sizes, InfNeRF and Nerfacto, theoretically, they should exhibit similar PSNR0. Our results confirm this hypothesis. As depicted along the horizontal axis of Fig. 6, InfNeRF slightly outperforms Nerfacto by 0.3 dB, demonstrating that InfNeRF’s octree partitioning and the limited memory requirement do not compromise the rendering quality. Furthermore, when considering results of multi-resolution rendering, plotted along the vertical axis, InfNeRF outperforms Nerfacto by 1.31 dB, PyNeRF by 1.01 dB and even outperform Mega-NeRF by 2.4 dB. This illustrates the crucial role of the LoD octree in anti-aliasing rendering. The same conclusion can be drawn from the quality comparison in Fig. 9. In the last three rows of each dataset, which display the low-resolution images, we can observe that without the anti-aliasing effect, Nerfacto and Mega-NeRF generate noisy results, particularly evident in the heavy moire pattern in the left bottom dataset solar panel region. In contrast, InfNeRF generates satisfactory results at both fine and coarse levels, showcasing its superiority in handling multi-resolution rendering. More detailed images are provided in Fig. 10.

4.2 Experiment On MipNeRF 360 Dataset

In addition to our previous large-scale experiment, we conduct another experiment with the garden scene of MipNeRF 360 Dataset. This smaller-scale scene allows us to evaluate and compare the performance of various methods. The following methods were included in our comparison: (1) Gaussian Splatting [Kerbl et al. 2023], (2) Mip-Splatting [Yu et al. 2024], (3) Nerfacto [Tancik et al. 2023], (4) PyNeRF [Turki et al. 2023]. All NeRF based methods have similar model size. More details of the experiment setting can be found in the supplementary material. As shown in Table. 2, InfNeRF exhibits competitive outcomes in high-resolution when compared to 3DGS [Kerbl et al. 2023] and Mip-Splatting [Yu et al. 2024]. It surpasses PyNeRF and Nerfacto by a margin of 3 dB. As the resolution decreases, 3DGS [Kerbl et al. 2023] and Nerfacto’s performance start to drop. Although anti-aliasing may not be the primary focus of InfNeRF, it consistently delivers commendable results without any additional computational cost.

4.3 Ablation Study

Table. 2 also includes an ablation study of our model on garden scene. (1) The transparency loss, improves slightly PSNR, and more importantly, removes the fog blocking the bird eyes view, as shown in Fig. 8. (2) Sampling radius perturbation not only smooth the transition between different LOD levels in some dataset, as depicted in Fig. 7, but also improve the overall PSNR. (3) Training without the upper tree structure, or (4) training without image pyramid, results in a significant reduction in PSNR at the low-resolution. (5) Removing one level of the tree reduces the model size by 4, and decreases the performance by 2 dB. (6) Tree pruning reduces the size of the tree to only 19 nodes, which accounted for only 26% of the full octree.

Table 1. Quantitative comparison on four public large-scale scene datasets. We report PSNR0 from full resolution and mean PSNR, SSIM, and LPIPS metrics from 6 resolutions. The **best results** are highlighted.

Scene Metric	Residential				Sci-Art				Rubble				Building			
	PSNR0 \uparrow	PSNR \uparrow	SSIM \uparrow	LPIPS \downarrow	PSNR0 \uparrow	PSNR \uparrow	SSIM \uparrow	LPIPS \downarrow	PSNR0 \uparrow	PSNR \uparrow	SSIM \uparrow	LPIPS \downarrow	PSNR0 \uparrow	PSNR \uparrow	SSIM \uparrow	LPIPS \downarrow
Nerfacto	24.32	24.31	0.772	0.216	26.75	26.48	0.827	0.182	24.99	26.09	0.692	0.336	22.53	22.94	0.663	0.325
PyNeRF	21.30	24.13	0.753	0.299	23.85	24.85	0.815	0.242	23.48	27.08	0.744	0.347	21.70	24.93	0.743	0.279
Mega-NeRF	22.52	22.85	0.748	0.265	24.37	24.22	0.808	0.202	24.17	26.02	0.73	0.294	21.70	22.43	0.696	0.282
InfNeRF-c	23.84	24.87	0.785	0.198	25.83	25.81	0.805	0.212	24.62	27.27	0.731	0.274	22.52	24.02	0.703	0.280
InfNeRF	24.66	25.46	0.820	0.158	27.03	26.96	0.839	0.192	25.12	27.92	0.781	0.203	23.11	24.70	0.740	0.242

Table 2. Quantitative comparison on garden scene from MipNeRF 360. We report PSNR at each scale.

Resolution	2 \times	4 \times	8 \times	16 \times	32 \times
Gaussian Splatting	26.52	25.18	21.58	19.01	17.266
Mip-Splatting	26.87	27.85	28.83	28.69	27.76
Nerfacto	23.18	23.5	24.08	23.32	22.09
PyNeRF	23.79	24.76	27.04	27.63	24.82
InfNeRF	26.27	27.04	28.2	28.87	27.23
(1) w/o Trans Loss	25.63	26.45	27.54	27.92	26.18
(2) w/o Perturbation	25.90	26.87	27.86	28.23	27.20
(3) w/o Upper Tree	24.71	25.22	24.95	24.02	22.69
(4) w/o Pyramid	26.12	23.04	13.00	8.98	8.52
(5) w 3 levels	24.78	25.2	26.2	27.26	25.96



Fig. 7. Left: in certain datasets, the absence of sampling sphere perturbation can lead to noticeable discontinuities between different levels of detail. Right: however, by incorporating perturbation in InfNeRF, these transitions are smoothed out, guaranteeing a seamless navigation experience.



Fig. 8. Left: the unobserved sky area is obscured by foggy artifacts, blocking the bird's-eye view. Right: transparency loss can effectively remove this artifact, allowing for a clearer and unobstructed bird's-eye view.

5 CONCLUSION AND FUTURE WORK

In this work, we introduce InfNeRF for large-scale scene reconstruction. InfNeRF employs an LoD tree to divide the scene in space and scale into cubes, which are reconstructed using many NeRFs. During rendering, InfNeRF selectively retrieves a minimal subset of

nodes, significantly reducing memory requirements and I/O time for parameter retrieval from disk or cloud storage and also reducing aliasing artifacts. In our experiments, InfNeRF achieves superior rendering quality, with an improvement of over 2.4 dB in PSNR while accessing only 17% of the total parameters.

InfNeRF demonstrates its potential for large-scale scene reconstruction. However, there are several aspects for future exploration and improvement. Firstly, the reconstruction time and computational burden still exceed traditional, well-optimized photogrammetry methods [DJI 2024; Schonberger and Frahm 2016], necessitating further performance enhancements. Secondly, exploring the combination of octree from diverse image sources, such as satellites, planes, and drones, at different times and scales, could enable the creation of larger scenes. With these works, digitizing the Earth using NeRF will become a compelling possibility for the future.

REFERENCES

- Jonathan T Barron, Ben Mildenhall, Matthew Tancik, Peter Hedman, Ricardo Martin-Brualla, and Pratul P Srinivasan. 2021. Mip-nerf: A multiscale representation for anti-aliasing neural radiance fields. In *Proceedings of the IEEE/CVF International Conference on Computer Vision*. 5855–5864.
- Jonathan T Barron, Ben Mildenhall, Dor Verbin, Pratul P Srinivasan, and Peter Hedman. 2022. Mip-nerf 360: Unbounded anti-aliased neural radiance fields. In *Proceedings of the IEEE/CVF Conference on Computer Vision and Pattern Recognition*. 5470–5479.
- Jonathan T Barron, Ben Mildenhall, Dor Verbin, Pratul P Srinivasan, and Peter Hedman. 2023. Zip-NeRF: Anti-aliased grid-based neural radiance fields. *arXiv preprint arXiv:2304.06706* (2023).
- Don Burns and Robert Osfield. 2004. Open scene graph a: Introduction, b: Examples and applications. In *Virtual Reality Conference, IEEE*. IEEE Computer Society, 265–265.
- Dan Cernea. 2020. OpenMVS: Multi-view stereo reconstruction library. *City* 5, 7 (2020).
- CesiumJS. 2024. *CesiumJS Homepage*. Retrieved Jan 20, 2024 from <https://cesium.com/>
- Eric R. Chan, Connor Z. Lin, Matthew A. Chan, Koki Nagano, Boxiao Pan, Shalini De Mello, Orazio Gallo, Leonidas Guibas, Jonathan Tremblay, Sameh Khamis, Tero Karras, and Gordon Wetzstein. 2022. Efficient Geometry-aware 3D Generative Adversarial Networks. In *CVPR*.
- Anpei Chen, Zexiang Xu, Andreas Geiger, Jingyi Yu, and Hao Su. 2022. TensorRF: Tensorial radiance fields. In *European Conference on Computer Vision*. Springer, 333–350.
- Zhiqin Chen, Thomas Funkhouser, Peter Hedman, and Andrea Tagliasacchi. 2023. Mobilenerf: Exploiting the polygon rasterization pipeline for efficient neural field rendering on mobile architectures. In *Proceedings of the IEEE/CVF Conference on Computer Vision and Pattern Recognition*. 16569–16578.
- James H Clark. 1976. Hierarchical geometric models for visible surface algorithms. *Commun. ACM* 19, 10 (1976), 547–554.
- Joel Daniels, Cláudio T Silva, Jason Shepherd, and Elaine Cohen. 2008. Quadrilateral mesh simplification. *ACM transactions on graphics (TOG)* 27, 5 (2008), 1–9.
- DJI. 2024. *Terra*. Retrieved Jan 20, 2024 from <https://enterprise.dji.com/dji-terra>
- Daniel Duckworth, Peter Hedman, Christian Reiser, Peter Zhizhin, Jean-François Thibert, Mario Lucić, Richard Szeliski, and Jonathan T. Barron. 2023. SMERF: Streamable Memory Efficient Radiance Fields for Real-Time Large-Scene Exploration. *arXiv:2312.07541* [cs.CV]
- Carl Erikson, Dinesh Manocha, and William V Baxter III. 2001. HLODs for faster display of large static and dynamic environments. In *Proceedings of the 2001 symposium on Interactive 3D graphics*. 111–120.

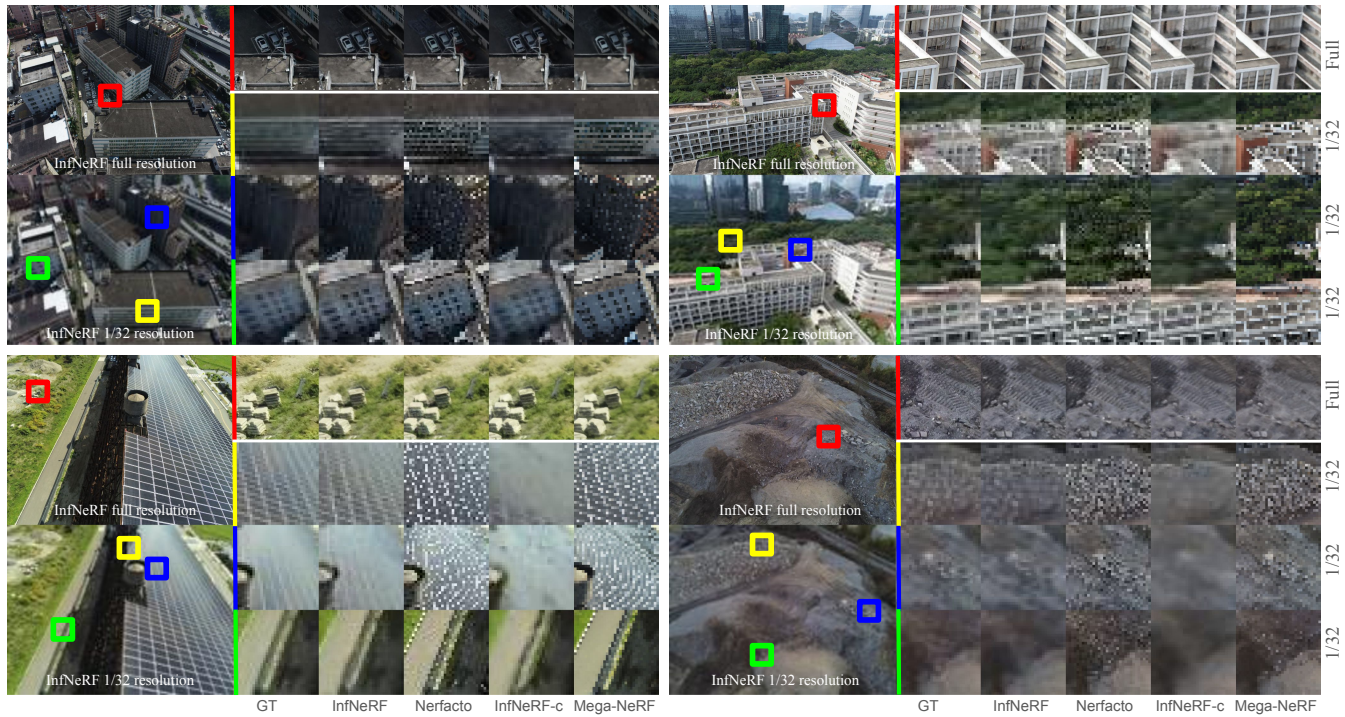


Fig. 9. Qualitative comparison between the baseline and InfNeRF on four public large-scale datasets reveals that the reduction of rendering model size do not harm the the rendering quality of InfNeRF at the highest resolution. Meanwhile Mega-NeRF appears blurry and fails to capture details effectively. In low resolution, both Mega-NeRF and Nerfacto suffer severe aliasing, particularly evident in moire patterns on the solar panel. Leveraging the LoD octree, InfNeRF not only captures most details in full resolution but also renders a smooth anti-aliasing image in low resolution.

Hugues Hoppe. 1998. Smooth view-dependent level-of-detail control and its application to terrain rendering. In *Proceedings Visualization '98 (Cat. No. 98CB36276)*. IEEE, 35–42.

Hugues Hoppe. 2023. Progressive meshes. In *Seminal Graphics Papers: Pushing the Boundaries, Volume 2*. 111–120.

Dongting Hu, Zhenkai Zhang, Tingbo Hou, Tongliang Liu, Huan Fu, and Mingming Gong. 2023b. Multiscale Representation for Real-Time Anti-Aliasing Neural Rendering. *arXiv preprint arXiv:2304.10075* (2023).

Wenbo Hu, Yuling Wang, Lin Ma, Bangbang Yang, Lin Gao, Xiao Liu, and Yuewen Ma. 2023a. Tri-miprf: Tri-mip representation for efficient anti-aliasing neural radiance fields. In *Proceedings of the IEEE/CVF International Conference on Computer Vision*. 19774–19783.

Bernhard Kerbl, Georgios Kopanas, Thomas Leimkühler, and George Drettakis. 2023. 3D Gaussian Splatting for Real-Time Radiance Field Rendering. *ACM Transactions on Graphics* 42, 4 (July 2023). <https://repo-sam.inria.fr/fungraph/3d-gaussian-splatting/>

Bernhard Kerbl, Andreas Meuleman, Georgios Kopanas, Michael Wimmer, Alexandre Lanvin, and George Drettakis. 2024. A Hierarchical 3D Gaussian Representation for Real-Time Rendering of Very Large Datasets. *ACM Transactions on Graphics* 43, 4 (July 2024). <https://repo-sam.inria.fr/fungraph/hierarchical-3d-gaussians/>

Jiaqi Lin, Zhihao Li, Xiao Tang, Jianzhuang Liu, Shiyong Liu, Jiayue Liu, Yangdi Lu, Xiaofei Wu, Songcen Xu, Youliang Yan, et al. 2024. Vastgaussian: Vast 3d gaussians for large scene reconstruction. In *Proceedings of the IEEE/CVF Conference on Computer Vision and Pattern Recognition*. 5166–5175.

Liqiang Lin, Yilin Liu, Yue Hu, Xingguang Yan, Ke Xie, and Hui Huang. 2022. Capturing, Reconstructing, and Simulating: the UrbanScene3D Dataset. In *ECCV*. 93–109.

Yang Liu, He Guan, Chuanchen Luo, Lue Fan, Junran Peng, and Zhaoxiang Zhang. 2024. Citygaussian: Real-time high-quality large-scale scene rendering with gaussians. *arXiv preprint arXiv:2404.01133* (2024).

David Luebke. 2003. *Level of detail for 3D graphics*. Morgan Kaufmann.

Ricardo Martin-Brualla, Noha Radwan, Mehdi S. M. Sajjadi, Jonathan T. Barron, Alexey Dosovitskiy, and Daniel Duckworth. 2021. NeRF in the Wild: Neural Radiance Fields for Unconstrained Photo Collections. In *CVPR*.

Ben Mildenhall, Pratul P Srinivasan, Matthew Tancik, Jonathan T Barron, Ravi Ramamoorthi, and Ren Ng. 2021. Nerf: Representing scenes as neural radiance fields for view synthesis. *Commun. ACM* 65, 1 (2021), 99–106.

Thomas Müller, Alex Evans, Christoph Schied, and Alexander Keller. 2022. Instant neural graphics primitives with a multiresolution hash encoding. *ACM Transactions on Graphics (ToG)* 41, 4 (2022), 1–15.

Christian Reiser, Rick Szeliski, Dor Verbin, Pratul Srinivasan, Ben Mildenhall, Andreas Geiger, Jon Barron, and Peter Hedman. 2023. Merf: Memory-efficient radiance fields for real-time view synthesis in unbounded scenes. *ACM Transactions on Graphics (TOG)* 42, 4 (2023), 1–12.

José Ribelles, Angeles López, and Oscar Belmonte. 2010. An Improved Discrete Level of Detail Model Through an Incremental Representation. In *TPCG*. 59–66.

Johannes L Schonberger and Jan-Michael Frahm. 2016. Structure-from-motion revisited. In *Proceedings of the IEEE conference on computer vision and pattern recognition*. 4104–4113.

Towaki Takikawa, Joey Litalien, Kangxue Yin, Karsten Kreis, Charles Loop, Derek Nowrouzezahrai, Alec Jacobson, Morgan McGuire, and Sanja Fidler. 2021. Neural geometric level of detail: Real-time rendering with implicit 3d shapes. In *Proceedings of the IEEE/CVF Conference on Computer Vision and Pattern Recognition*. 11358–11367.

Matthew Tancik, Vincent Casser, Xinchen Yan, Sabeek Pradhan, Ben Mildenhall, Pratul P Srinivasan, Jonathan T Barron, and Henrik Kretzschmar. 2022. Block-nerf: Scalable large scene neural view synthesis. In *Proceedings of the IEEE/CVF Conference on Computer Vision and Pattern Recognition*. 8248–8258.

Matthew Tancik, Ethan Weber, Evonne Ng, Ruilong Li, Brent Yi, Justin Kerr, Terrance Wang, Alexander Kristoffersen, Jake Austin, Kamyar Salahi, Abhik Ahuja, David McAllister, and Angjoo Kanazawa. 2023. Nerfstudio: A Modular Framework for Neural Radiance Field Development. In *ACM SIGGRAPH 2023 Conference Proceedings (SIGGRAPH '23)*.

Christopher C Tanner, Christopher J Migdal, and Michael T Jones. 1998. The clipmap: a virtual mipmap. In *Proceedings of the 25th annual conference on Computer graphics and interactive techniques*. 151–158.

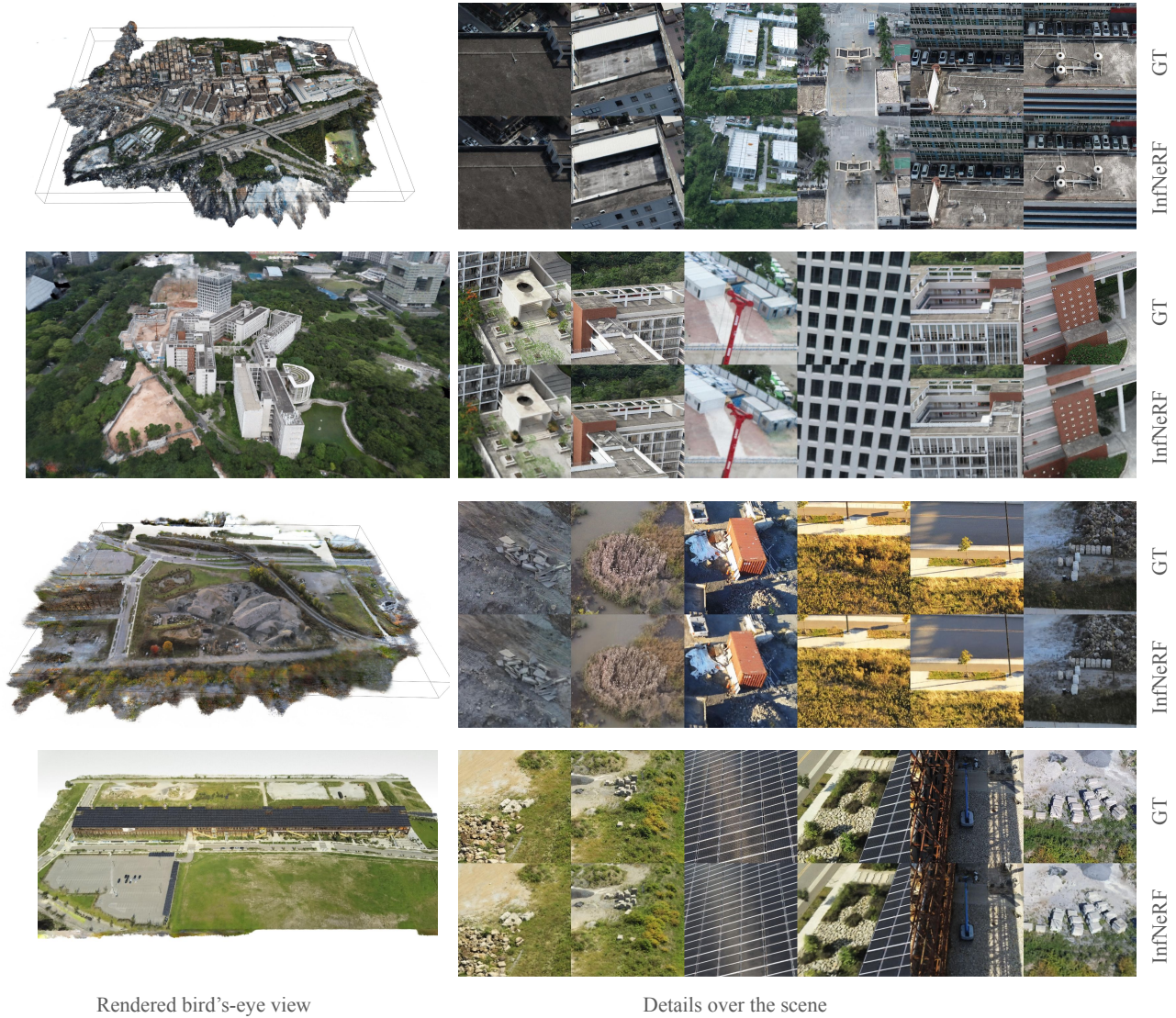


Fig. 10. Left: The bird’s-eye view showcases four large-scale scenes reconstructed by InfNeRF. Right: The detailed view provides a closer look at certain corner of the scene. InfNeRF demonstrates its ability to reconstruct large-scale scenes while preserving high quality and capturing intricate details.

Tiled web map. 2024. *Tiled web map*— *Wikipedia, The Free Encyclopedia*. Retrieved Jan 20, 2024 from https://en.wikipedia.org/wiki/Tiled_web_map

Haithem Turki, Deva Ramanan, and Mahadev Satyanarayanan. 2022. Mega-nerf: Scalable construction of large-scale nerfs for virtual fly-throughs. In *Proceedings of the IEEE/CVF Conference on Computer Vision and Pattern Recognition*. 12922–12931.

Haithem Turki, Michael Zollhöfer, Christian Richardt, and Deva Ramanan. 2023. PyNeRF: Pyramidal Neural Radiance Fields. *arXiv preprint arXiv:2312.00252* (2023).

Thatcher Ulrich. 2002. Rendering massive terrains using chunked level of detail control. In *Proc. ACM SIGGRAPH 2002*.

Lance Williams. 1983. Pyramidal parametrics. In *Proceedings of the 10th annual conference on Computer graphics and interactive techniques*. 1–11.

Xiuchao Wu, Jiamin Xu, Xin Zhang, Hujun Bao, Qixing Huang, Yujun Shen, James Tompkin, and Weiwei Xu. 2023. ScaNeRF: Scalable Bundle-Adjusting Neural Radiance Fields for Large-Scale Scene Rendering. *ACM Transactions on Graphics (TOG)* 42, 6 (2023), 1–18.

Yuanbo Xiangli, Linning Xu, Xingang Pan, Nanxuan Zhao, Anyi Rao, Christian Theobalt, Bo Dai, and Dahua Lin. 2022. Bungeenerf: Progressive neural radiance field for extreme multi-scale scene rendering. In *European conference on computer vision*. Springer, 106–122.

Linning Xu, Yuanbo Xiangli, Sida Peng, Xingang Pan, Nanxuan Zhao, Christian Theobalt, Bo Dai, and Dahua Lin. 2023. Grid-guided Neural Radiance Fields for Large Urban Scenes. In *Proceedings of the IEEE/CVF Conference on Computer Vision and Pattern Recognition*. 8296–8306.

Alex Yu, Ruilong Li, Matthew Tancik, Hao Li, Ren Ng, and Angjoo Kanazawa. 2021. Plenotrees for real-time rendering of neural radiance fields. In *Proceedings of the IEEE/CVF International Conference on Computer Vision*. 5752–5761.

Zehao Yu, Anpei Chen, Binbin Huang, Torsten Sattler, and Andreas Geiger. 2024. Mip-splatting: Alias-free 3d gaussian splatting. In *Proceedings of the IEEE/CVF Conference on Computer Vision and Pattern Recognition*. 19447–19456.